

Bias-Hardened CMB Lensing with Polarization

Toshiya Namikawa^{1*} and Ryuichi Takahashi²

¹*Yukawa Institute for Theoretical Physics, Kyoto University, Kyoto 606-8502, Japan*

²*Faculty of Science and Technology, Hirosaki University, 3 bunkyo-cho, Hirosaki, Aomori, 036-8561, Japan*

10 June 2019

ABSTRACT

Polarization data will soon provide the best avenue for measurements of the CMB lensing potential, although it is potentially sensitive to several instrumental effects including beam asymmetry, polarization angle uncertainties, sky coverage, as well as analysis choices such as masking. We derive “bias-hardened” lensing estimators to mitigate these effects, at the expense of somewhat larger reconstruction noise, and test them numerically on simulated data. We find that the mean-field bias from masking is significant for the EE quadratic lensing estimator, however the bias-hardened estimator combined with filtering techniques can mitigate the mean field. On the other hand, the EB estimator does not significantly suffer from the mean-field from the point source masking and survey window function. The contamination from beam asymmetry and polarization angle uncertainties, however, can generate mean-field biases for the EB estimator. These can also be mitigated using bias-hardened estimators, with at most a factor of ~ 3 degradation of noise level compared to the conventional approach.

Key words: gravitational lensing; weak – cosmic microwave background – cosmology; observations.

1 INTRODUCTION

On arcminute scales, the CMB temperature and polarization anisotropies are distorted by gravitational lensing. For the past several years, CMB observations have been used to make increasingly precise measurements of this effect, both with cross-correlations between CMB and large-scale structure (Smith et al. 2007; Hirata et al. 2008; Bleem et al. 2012; Sherwin et al. 2012; Planck Collaboration 2013c; Holder et al. 2013; Geach et al. 2013; Hanson et al. 2013) as well as CMB maps alone (Das et al. 2011; van Engelen et al. 2012; Das et al. 2013; Planck Collaboration 2013b; Hanson et al. 2013).

These lensing measurements are already being used to constrain cosmology (e.g., Sherwin et al. 2011; van Engelen et al. 2012; Planck Collaboration 2013a; Battye & Moss 2013; Namikawa et al. 2013; Wilkinson et al. 2013), future measurements are expected to quantify the sum of neutrino masses (e.g., Namikawa et al. 2010; Joudaki & Kaplinghat 2012; Abazajian et al. 2013 and refs. therein), and provide even tighter constraints on cosmic strings (e.g., Namikawa et al. 2012; Yamauchi et al. 2012, 2013), primordial non-Gaussianity (e.g., Jeong et al. 2009; Takeuchi et al. 2012), and other fundamental physics. Lensing potential estimates should also be important for *delensing* (Knox & Song 2002;

Kesden et al. 2002) to detect inflationary gravitational waves at > 10 if the tensor-to-scalar ratio is less than $r \sim 0.01$.

Given an observed CMB, estimators to reconstruct the lensing potential have been derived by several authors (e.g., Zaldarriaga & Seljak 1999; Seljak & Zaldarriaga 1999; Hu & Okamoto 2002; Okamoto & Hu 2003; Hirata & Seljak 2003; Namikawa et al. 2012). These estimators all utilize the fact that a fixed lensing potential introduces statistical anisotropy into the observed CMB, in the form of a correlation between the CMB temperature/polarization anisotropies and their gradients. With a large number of observed CMB modes, this correlation may be used to form estimates of the lensing potential. The power spectrum of the lensing potential, which is of more interest for cosmological parameter constraints, can then be estimated from the power spectrum of these estimates (which probes the non-Gaussian 4-point function of the lensed CMB). For CMB observations with noise levels below $5\mu K \cdot \text{arcmin}$, B -mode polarization is a particularly powerful probe of lensing as it is believed to be dominated by the lensing contribution on scales $\gtrsim 100$.

For realistic CMB observations, there are so called *mean-field biases* for the standard minimum-variance quadratic lensing estimators due to non-lensing sources of statistical anisotropy such as masking, inhomogeneous map noise, beam asymmetry, or spatially-varying errors in the detector polarization angles. With perfect statistical understanding of the unlensed CMB and the instrument used to

* E-mail: namikawa@yukawa.kyoto-u.ac.jp

observe it, these biases may be corrected for, however given imperfections in our understanding of these quantities it can be useful to design estimators which are less sensitive to them.

Approaches have been proposed in the literature to mitigate some of the mean-field biases. The mean fields from masking in temperature, for example, have been studied by several authors, with approaches including simply avoiding mask boundaries (Hirata et al. 2008; Carvalho & Tereno 2011), or using inpainting/apodization (Perotto et al. 2010; Plaszczynski et al. 2012; Benoit-Levy et al. 2013) to smooth them. These techniques could also be utilized for polarization, in conjunction with “pure” estimators for E and B modes (Smith 2006; Smith & Zaldarriaga 2007). For temperature case, the mean-field bias from inhomogeneous map noise is also studied in Hanson et al. (2009).

In this paper, we extend the bias-hardened estimators proposed in our previous work (Namikawa et al. 2013) to the case of lensing reconstruction with polarization, constructing lensing estimators which can have significantly smaller mean-field biases than the standard minimum-variance estimators, with minimal loss of signal-to-noise.

This paper is organized as follows. In Sec. 2, we briefly summarize quadratic estimators for the lensing potential using CMB temperature and polarization. In Sec. 3, we discuss several possible mean-field biases which must be corrected for, and then construct corresponding bias-hardened estimators. In Sec. 4, we demonstrate the usefulness of bias-hardened estimators using numerical simulations. Sec. 5 summarizes our results.

Finally, we note that when estimating the power spectrum of the lensing potential, there is an additional worrisome bias, the *reconstruction noise* bias, which must be accounted for. This bias is analogous to shape-noise in galaxy weak lensing measurements; in principle it can be avoided by forming independent lensing estimates from subsets of the observed sky modes, for example using an odd/even parity split (Hu 2001) or the in/out Fourier split (Sherwin & Das 2010). There is, however, usually a substantial loss of signal-to-noise associated with such splits. This bias is less of an issue in polarization than in temperature, because it falls with the instrumental noise level for estimates which utilize B -mode polarization, and can also be avoided using cross-spectra between different lensing estimates. In appendix A we present a polarized derivation of the optimal trispectrum-estimator approach to correcting for this bias, also extending our discussion of this approach for the temperature case in (Namikawa et al. 2013).

2 QUADRATIC LENSING RECONSTRUCTION FROM CMB MAPS

2.1 Lensing effect on CMB anisotropies

The distortion effect of lensing on the primary temperature and polarization anisotropies is expressed by a remapping of the primary anisotropies. Denoting the primary CMB anisotropies at position $\hat{\mathbf{n}} = (\theta, \varphi)$ on the last scattering surface as $\Xi^{(s)}(\hat{\mathbf{n}})$, where $s = 0$ denotes the temperature, $\Xi^{(0)} = \Theta$, while $s = \pm 2$ are the spin-2 combination of the Stokes parameter, $\Xi^{(\pm 2)} = Q \pm iU \equiv P^\pm$, the lensed

Table 1. The weight functions for lensing potentials, $f_{\ell, \mathbf{L}}^{x, (XY)}$. Note that $\mathbf{L}' = \ell - \mathbf{L}$.

Lensing	
$\Theta\Theta$	$c_x^{ab} \{\ell_a L_b \tilde{C}_L^{\Theta\Theta} + \ell_a L'_b \tilde{C}_{L'}^{\Theta\Theta}\}$
ΘE	$c_x^{ab} \{\ell_a L_b \tilde{C}_L^{\Theta E} \cos 2\varphi_{\mathbf{L}, \mathbf{L}'} + \ell_a L'_b \tilde{C}_{L'}^{\Theta E}\}$
ΘB	$c_x^{ab} \{\ell_a L_b \tilde{C}_L^{\Theta E} \sin 2\varphi_{\mathbf{L}, \mathbf{L}'}\}$
EE	$c_x^{ab} \{\ell_a L_b \tilde{C}_L^{EE} + \ell_a L'_b \tilde{C}_{L'}^{EE}\} \cos 2\varphi_{\mathbf{L}, \mathbf{L}'}$
EB	$c_x^{ab} \{\ell_a L_b \tilde{C}_L^{EE} + \ell_a L'_b \tilde{C}_{L'}^{BB}\} \sin 2\varphi_{\mathbf{L}, \mathbf{L}'}$
BB	$c_x^{ab} \{\ell_a L_b \tilde{C}_L^{BB} + \ell_a L'_b \tilde{C}_{L'}^{BB}\} \cos 2\varphi_{\mathbf{L}, \mathbf{L}'}$

anisotropies in a direction $\hat{\mathbf{n}}$, are given by (e.g., Lewis & Challinor 2006)

$$\begin{aligned} \tilde{\Xi}^{(s)}(\hat{\mathbf{n}}) &= \Xi^{(s)}(\hat{\mathbf{n}} + \mathbf{d}(\hat{\mathbf{n}})) \\ &= \Xi^{(s)}(\hat{\mathbf{n}}) + d^a(\hat{\mathbf{n}}) \partial_a \Xi^{(s)}(\hat{\mathbf{n}}) + \mathcal{O}(|\mathbf{d}|^2). \end{aligned} \quad (1)$$

The two-dimensional vector, $d^a(\hat{\mathbf{n}})$ ($a = \theta, \varphi$), is the deflection angle, and, in terms of parity symmetry, we can decompose it into two terms, known as gradient (even parity) and curl (odd parity) modes (e.g., Hirata & Seljak 2003; Cooray et al. 2005; Namikawa et al. 2012):

$$d^a(\hat{\mathbf{n}}) = \partial^a \phi(\hat{\mathbf{n}}) + \epsilon^{ab} \partial_b \varpi(\hat{\mathbf{n}}) = \sum_{x=\phi, \varpi} c_x^{ab} \partial_b x(\hat{\mathbf{n}}), \quad (2)$$

where the symbol, c_ϕ^{ab} , is the Kronecker delta and $c_\varpi^{ab} = \epsilon^{ab}$ is the two-dimensional Levi-Civita symbol.

2.2 Estimator for lensing fields

The temperature anisotropies are distorted by lensing as (e.g., Hu & Okamoto 2002)¹

$$\tilde{\Theta}_\ell = \Theta_\ell - \sum_{x=\phi, \varpi} \int \frac{d^2 \mathbf{L}}{(2\pi)^2} c_x^{ab} L_a (b - L_b) \phi_L \Theta_{\ell - \mathbf{L}}. \quad (5)$$

On the other hand, for polarization we usually use the rotationally invariant combination, i.e., the E and B mode polarizations, instead of the spin-2 quantity (e.g., Hu & Okamoto 2002):

$$E_\ell \pm iB_\ell = - \int d^2 \hat{\mathbf{n}} e^{-i\hat{\mathbf{n}} \cdot \ell} P^\pm(\hat{\mathbf{n}}) e^{\mp 2i\varphi_\ell}, \quad (6)$$

where φ_ℓ is the angle of ℓ measured from the x -axis. With deflection angle given in Eq. (2), the lensed E and B modes

¹ Our definitions of Fourier transform and its inverse for arbitrary quantity $X(\hat{\mathbf{n}})$ on a map are

$$X_\ell = \int d^2 \hat{\mathbf{n}} e^{-i\hat{\mathbf{n}} \cdot \ell} X(\hat{\mathbf{n}}), \quad (3)$$

$$X(\hat{\mathbf{n}}) = \int \frac{d^2 \ell}{(2\pi)^2} e^{i\ell \cdot \hat{\mathbf{n}}} X_\ell. \quad (4)$$

These are the same as Hu & Okamoto (2002) but different from, e.g., Lewis & Challinor (2006).

are given by (e.g., Hu & Okamoto 2002; Cooray et al. 2005; Namikawa et al. 2012)

$$\tilde{E}_\ell = E_\ell - \int \frac{d^2 \mathbf{L}}{(2\pi)^2} (L^a L'_a \phi_{\mathbf{L}} + \epsilon^{ab} L_a L'_b \varpi_\ell) \times (E_{\mathbf{L}'} \cos 2\varphi_{\mathbf{L}',\ell} - B_{\mathbf{L}'} \sin 2\varphi_{\mathbf{L}',\ell}), \quad (7)$$

$$\tilde{B}_\ell = B_\ell - \int \frac{d^2 \mathbf{L}}{(2\pi)^2} (L^a L'_a \phi_{\mathbf{L}} + \epsilon^{ab} L_a L'_b \varpi_\ell) \times (B_{\mathbf{L}'} \cos 2\varphi_{\mathbf{L}',\ell} + E_{\mathbf{L}'} \sin 2\varphi_{\mathbf{L}',\ell}), \quad (8)$$

with $\mathbf{L}' = \ell - \mathbf{L}$ and $\varphi_{\ell_1, \ell_2} \equiv \varphi_{\ell_1} - \varphi_{\ell_2}$.

Denoting X and Y as Θ , E or B , the off-diagonal covariance includes the gradient and curl modes of deflections as

$$\langle \tilde{X}_{\mathbf{L}} \tilde{Y}_{\mathbf{L}'} \rangle_{\text{CMB}} = f_{\ell, \mathbf{L}}^{x, (XY)} x_\ell, \quad (9)$$

where $\langle \dots \rangle_{\text{CMB}}$ denotes the ensemble average over unlensed Θ , E or B , with a fixed realization of the gradient and curl modes, and we ignore the higher-order terms of lensing fields. The weight functions for gradient and curl modes are summarized in Table 1 (Hu & Okamoto 2002; Cooray et al. 2005; Namikawa et al. 2012). Note that, to mitigate the higher-order biases (Hanson et al. 2011), the lensed power spectrum is used rather than the unlensed one (Lewis et al. 2011; Anderes 2013): With a quadratic combination of X and Y fluctuations, the lensing estimators are then formed as (e.g., Hu & Okamoto 2002),

$$\hat{x}_\ell^{(XY)} = \frac{1}{2} A_\ell^{x, (XY)} \int \frac{d^2 \mathbf{L}}{(2\pi)^2} g_{\ell, \mathbf{L}}^{x, (XY)} \overline{X}_{\mathbf{L}} \overline{Y}_{\mathbf{L}'}, \quad (10)$$

where, with the ratio of power spectra, $r_L^{XY} = \hat{C}_L^{XY} / \hat{C}_L^{XX}$, we define²

$$g_{\ell, \mathbf{L}}^{x, (XY)} = 2 \frac{[f_{\ell, \mathbf{L}}^{x, (XY)}]^* - r_L^{XY} r_{\mathbf{L}'}^{YX} [f_{\ell, \mathbf{L}'}^{x, (XY)}]^*}{1 - r_L^{XY} r_{\mathbf{L}'}^{XY} r_{\mathbf{L}}^{YX} r_{\mathbf{L}'}^{XX}}, \quad (11)$$

$$A_\ell^{x, (XY)} = \left\{ \int \frac{d^2 \mathbf{L}}{(2\pi)^2} \frac{g_{\ell, \mathbf{L}}^{x, (XY)} f_{\ell, \mathbf{L}}^{x, (XY)}}{2 \hat{C}_L^{XX} \hat{C}_{\mathbf{L}'}^{YY}} \right\}^{-1}. \quad (12)$$

The inverse-variance filtered Fourier modes are given by

$$\overline{X}_\ell = \frac{\hat{X}_\ell}{\hat{C}_\ell^{XX}}. \quad (13)$$

For the cosmic variance case, the estimated power spectrum reduces to the lensed power spectrum.

3 BIAS-HARDENED LENSING ESTIMATORS

There are many effects which can generate mode-coupling between observed Θ , E and B modes, leading to mean-field biases for the conventional lensing estimators. In the following, we compute the non-lensing statistical anisotropy due to masking, inhomogeneous noise (and/or unresolved point sources), and polarization angle (or scan strategy) systematics in the presence of beam asymmetry. Then, in order to mitigate the mean-field biases from these systematics, we construct bias-hardened estimator analogous to those of our previous work (Namikawa et al. 2013).

² Note here that the normalization, $A_\ell^{x, (XY)}$, is independent of the direction of ℓ , so we write the normalization as $A_\ell^{x, (XY)}$.

Table 2. The weight functions for masking, $f_{\ell, \mathbf{L}}^{M, (XY)}$. Note that $\mathbf{L}' = \ell - \mathbf{L}$.

Masking	
$\Theta\Theta$	$-\tilde{C}_L^{\Theta\Theta} - \tilde{C}_{\mathbf{L}'}^{\Theta\Theta}$
ΘE	$-\tilde{C}_L^{\Theta E} \cos 2\varphi_{\mathbf{L}, \mathbf{L}'} - \tilde{C}_{\mathbf{L}'}^{\Theta E}$
ΘB	$-\tilde{C}_L^{\Theta E} \sin 2\varphi_{\mathbf{L}, \mathbf{L}'}$
EE	$-(\tilde{C}_L^{EE} + \tilde{C}_{\mathbf{L}'}^{EE}) \cos \varphi_{\mathbf{L}, \mathbf{L}'}$
EB	$-(\tilde{C}_L^{EE} + \tilde{C}_{\mathbf{L}'}^{BB}) \sin \varphi_{\mathbf{L}, \mathbf{L}'}$
BB	$-(\tilde{C}_L^{BB} + \tilde{C}_{\mathbf{L}'}^{BB}) \cos \varphi_{\mathbf{L}, \mathbf{L}'}$

3.1 Non-lensing sources in the off-diagonal covariance

3.1.1 Masking

Let us first consider the modification due to a window function, $M(\hat{\mathbf{n}})$, which is defined to be zero for an unmasked region and otherwise unity:

$$\hat{\Theta}(\hat{\mathbf{n}}) = [1 - M(\hat{\mathbf{n}})] \tilde{\Theta}(\hat{\mathbf{n}}), \quad (14)$$

$$\hat{P}^\pm(\hat{\mathbf{n}}) = [1 - M(\hat{\mathbf{n}})] \tilde{P}^\pm(\hat{\mathbf{n}}). \quad (15)$$

Such masking mixes E and B modes, leading to mode-coupling in temperature and polarization as

$$\hat{\Theta}_\ell = \tilde{\Theta}_\ell - \int \frac{d^2 \mathbf{L}}{(2\pi)^2} M_{\mathbf{L}} \tilde{\Theta}_{\mathbf{L}'}, \quad (16)$$

$$\hat{E}_\ell = \tilde{E}_\ell - \int \frac{d^2 \mathbf{L}}{(2\pi)^2} M_{\mathbf{L}} \left\{ \tilde{E}_{\mathbf{L}'} \cos \varphi_{\mathbf{L}', \mathbf{L}} - \tilde{B}_{\mathbf{L}'} \sin \varphi_{\mathbf{L}', \mathbf{L}} \right\}, \quad (17)$$

$$\hat{B}_\ell = \tilde{B}_\ell - \int \frac{d^2 \mathbf{L}}{(2\pi)^2} M_{\mathbf{L}} \left\{ \tilde{B}_{\mathbf{L}'} \cos \varphi_{\mathbf{L}', \mathbf{L}} + \tilde{E}_{\mathbf{L}'} \sin \varphi_{\mathbf{L}', \mathbf{L}} \right\}. \quad (18)$$

With the above equations, the resultant off-diagonal covariance can be written as

$$\langle \hat{X}_{\mathbf{L}} \hat{Y}_{\mathbf{L}'} \rangle = M_\ell f_{\ell, \mathbf{L}}^{M, (XY)} + \mathcal{O}(M^2), \quad (19)$$

where $\langle \dots \rangle$ denotes the usual ensemble average, and the weight functions are summarized in Table 2. The above equation implies that the resultant lensing estimator has the mean-field bias due to the mask field, M_ℓ .

3.1.2 Inhomogeneous noise/unresolved point-source

Let us next consider the modification due to addition of arbitrary sky signals, $n^T(\hat{\mathbf{n}})$, $n^Q(\hat{\mathbf{n}})$ and $n^U(\hat{\mathbf{n}})$, which are uncorrelated between pixels – this approach can be used to model, e.g., residual point sources and inhomogeneous instrumental noise in temperature and polarization maps. The corresponding Θ , E and B modes are given by

$$n_\ell^\Theta = \int d^2 \hat{\mathbf{n}} e^{-i\hat{\mathbf{n}} \cdot \ell} n^T(\hat{\mathbf{n}}), \quad (20)$$

$$n_\ell^E \pm i n_\ell^B = \int d^2 \hat{\mathbf{n}} e^{-i\hat{\mathbf{n}} \cdot \ell} [n^Q \pm i n^U](\hat{\mathbf{n}}) e^{\mp 2i\varphi_\ell}. \quad (21)$$

Table 3. Same as Table 2, but for polarization angle, $f_{\ell, \mathbf{L}}^{\psi^{(n,p)}, (XY)}$. For clarity, the exponential is expressed as “exp”.

$p = 0$	
$\Theta\Theta$	$[\mathcal{B}_{L, (n,0)}^{(\Theta\Theta)} \tilde{C}_L^{\Theta\Theta} + \mathcal{B}_{L, (n,0)}^{(\Theta E)} \tilde{C}_L^{\Theta E}] \exp(i n \varphi_{-L, \ell}) + (\mathbf{L} \leftrightarrow \mathbf{L}')$
ΘE	$[\mathcal{B}_{L', (n,0)}^{(\Theta\Theta)} \tilde{C}_{L'}^{\Theta E} + \mathcal{B}_{L', (n,0)}^{(\Theta E)} \tilde{C}_{L'}^{EE}] \exp(i n \varphi_{-L', \ell})$
ΘB	$\mathcal{B}_{L', (n,0)}^{(\Theta B)} \tilde{C}_{L'}^{BB} \exp(i n \varphi_{-L', \ell})$
EE	0
EB	0
BB	0
$p = \pm 1$	
$\Theta\Theta$	0
ΘE	$[\mathcal{B}_{L, (n,p)}^{(E\Theta)} \tilde{C}_L^{\Theta\Theta} + \mathcal{B}_{L, (n,p)}^{(EE)} \tilde{C}_L^{\Theta E}] \exp(i n \varphi_{-L, \ell} \pm 2i \varphi_{-L, L'})$
ΘB	$[\mathcal{B}_{L, (n,p)}^{(B\Theta)} \tilde{C}_L^{\Theta\Theta} + \mathcal{B}_{L, (n,p)}^{(BE)} \tilde{C}_L^{\Theta E}] \exp(i n \varphi_{-L, \ell} \pm 2i \varphi_{-L, L'})$
EE	$[\mathcal{B}_{L, (n,p)}^{(E\Theta)} \tilde{C}_L^{\Theta E} + \mathcal{B}_{L, (n,p)}^{(EE)} \tilde{C}_L^{EE}] \exp(i n \varphi_{-L, \ell} \pm 2i \varphi_{-L, L'}) + (\mathbf{L} \leftrightarrow \mathbf{L}')$
EB	$[\mathcal{B}_{L, (n,p)}^{(B\Theta)} \tilde{C}_L^{\Theta E} + \mathcal{B}_{L, (n,p)}^{(BE)} \tilde{C}_L^{EE}] \exp(i n \varphi_{-L, \ell} \pm 2i \varphi_{-L, L'}) + \mathcal{B}_{L', (n,p)}^{(EB)} \tilde{C}_{L'}^{BB} \exp(i n \varphi_{-L', \ell} \pm 2i \varphi_{-L', L'})$
BB	$\mathcal{B}_{L, (n,p)}^{(BB)} \tilde{C}_L^{BB} \exp(i n \varphi_{-L, \ell} \pm 2i \varphi_{-L, L'}) + (\mathbf{L} \leftrightarrow \mathbf{L}')$

Assuming that $\langle n^X(\hat{\mathbf{n}}) n^Y(\hat{\mathbf{n}}') \rangle = S^{(X)}(\hat{\mathbf{n}}) \delta^{XY} \delta(\hat{\mathbf{n}} - \hat{\mathbf{n}}')$, $S^{\Theta U} = S^{\Theta U} = 0$ and $S^{(QQ)} = S^{(UU)} \equiv S^{(P)}$, we have

$$\begin{aligned} \langle n_L^{\Theta} n_{L'}^{\Theta} \rangle &= S_{\ell}^{(\Theta)}, \\ \langle n_L^E n_{L'}^E \rangle &= S_{\ell}^{(P)} \cos 2\varphi_{L, L'}, \\ \langle n_L^E n_{L'}^B \rangle &= S_{\ell}^{(P)} \sin 2\varphi_{L, L'}, \\ \langle n_L^B n_{L'}^B \rangle &= S_{\ell}^{(P)} \cos 2\varphi_{L, L'}, \end{aligned}$$

where we use $\mathbf{L} + \mathbf{L}' = \ell$ and define

$$S_{\ell}^{(X)} = \int d^2 \hat{\mathbf{n}} e^{-i \hat{\mathbf{n}} \cdot \ell} S^{(X)}(\hat{\mathbf{n}}). \quad (22)$$

The off-diagonal covariance then has additional terms

$$\langle \hat{X}_L \hat{Y}_{L'} \rangle = \langle n_L^X n_{L'}^Y \rangle = f_{\ell, \mathbf{L}}^{S, (XY)} S_{\ell}^{(X)}. \quad (23)$$

where the weight function is $f_{\ell, \mathbf{L}}^{S, (\Theta\Theta)} = 1$, $f_{\ell, \mathbf{L}}^{S, (EE)} = f_{\ell, \mathbf{L}}^{S, (BB)} = \cos 2\varphi_{L, L'}$, and $f_{\ell, \mathbf{L}}^{S, (EB)} = \sin 2\varphi_{L, L'}$.

3.1.3 Polarization angle with beam asymmetry

Instrumental effects such as beam asymmetry and errors in the detector polarization angles are also a potential concern for lensing reconstruction. Here we consider the effect of a spatial variation in the polarization angle in the presence of the ellipticity in beam shape.

Denoting CMB temperature and polarization anisotropies as $\Xi^{(0)} = \Theta$ and $\Xi^{(\pm 2)} = Q \pm iU = P^{\pm}$, we assume that the beam convolved anisotropies for the i -th pixel are expressed as follows:

$$\Xi^{(s)}(\hat{\mathbf{n}}_i) = \int d^2 \hat{\mathbf{n}} \mathcal{R}(\hat{\mathbf{n}}_i - \hat{\mathbf{n}}, \alpha(\hat{\mathbf{n}}_i)) \Xi^{(s)}(\hat{\mathbf{n}}), \quad (24)$$

where $s = 0$ (temperature) or ± 2 (polarization), and \mathcal{R}

denotes the beam-response function whose shape is independent of the measurements but whose orientation angle, $\alpha(\hat{\mathbf{n}}_i)$ (Shimon et al. 2008), is dependent on both the pixels and measurements. The beam-response function, \mathcal{R} , is given by

$$\mathcal{R}(\mathbf{r}, \alpha(\hat{\mathbf{n}}_i)) = \int \frac{d^2 \mathbf{L}}{(2\pi)^2} e^{i \mathbf{L} \cdot \mathbf{r}} \mathcal{R}_{\mathbf{L}}(\hat{\mathbf{n}}_i), \quad (25)$$

where the Fourier counterpart of the beam-response function is expanded as (Shimon et al. 2008)

$$\mathcal{R}_{\mathbf{L}}(\hat{\mathbf{n}}_i) = \sum_{n=-\infty}^{\infty} b_{L, n} e^{-i n \alpha(\hat{\mathbf{n}}_i)} e^{i n \varphi_{\mathbf{L}}}. \quad (26)$$

Here, by denoting the Bessel function as, J_n , the coefficients are given by

$$b_{L, n} = i^n \int d\mathbf{r} r J_n(Lr) \int \frac{d\varphi_r}{2\pi} \mathcal{R}(\mathbf{r}, 0) e^{-i n \varphi_r}. \quad (27)$$

Note that $b_{L, -n} = (-1)^n b_{L, n}$, and if the shape of beam function, $\mathcal{R}(\mathbf{r}, 0)$, does not depend on the angle, φ_r , e.g., a circular Gaussian beam, the coefficients are non-zero only when $n = 0$. The beam-convolved anisotropies are then rewritten as

$$\begin{aligned} \Xi^{(s)}(\hat{\mathbf{n}}_i) &= i^s \sum_{n=-\infty}^{\infty} e^{-i n \alpha(\hat{\mathbf{n}}_i)} \\ &\times \int \frac{d^2 \mathbf{L}}{(2\pi)^2} b_{L, n} \Xi_{\mathbf{L}}^{(s)} e^{i \mathbf{L} \cdot \hat{\mathbf{n}}_i} e^{i (n+s) \varphi_{\mathbf{L}}}, \end{aligned} \quad (28)$$

where $\Xi^{(0)} = \Theta$ and $\Xi^{(\pm 2)} = E \pm iB$.

For a two-beam experiment, as shown in Shimon et al. (2008), the measured temperature and polarization anisotropies are distorted by the polarization angle and difference of beam shapes between the first and second detector. If the anisotropies are measured several times at each

pixel, the optimal estimators for temperature and polarization anisotropies are given by (Shimon et al. 2008)

$$\begin{aligned} \hat{\Xi}^{(0)} &= \langle \Xi_+^{(0)} \rangle_{\text{pix}} + \frac{1}{2} \langle \Xi_-^{(-2)} e^{2i\hat{\alpha}_t} e^{-2i\delta_t} \rangle_{\text{pix}} \\ &\quad + \frac{1}{2} \langle \Xi_-^{(+2)} e^{-2i\hat{\alpha}_t} e^{2i\delta_t} \rangle_{\text{pix}}, \end{aligned} \quad (29)$$

$$\begin{aligned} \hat{\Xi}^{(\pm 2)} &= \langle \Xi_+^{(\pm 2)} e^{\pm 2i\delta_t} \hat{\Psi}_t^{\pm} \rangle_{\text{pix}} + \langle \Xi_+^{(\mp 2)} e^{\mp 2i\delta_t} e^{\pm 4i\hat{\alpha}_t} \hat{\Psi}_t^{\pm} \rangle_{\text{pix}} \\ &\quad + 2 \langle \Xi_-^{(0)} e^{\pm 2i\hat{\alpha}_t} \hat{\Psi}_t^{\pm} \rangle_{\text{pix}}, \end{aligned} \quad (30)$$

where the arguments, $\hat{\mathbf{n}}_i$, are dropped. The bracket, $\langle \cdots \rangle_{\text{pix}}$, denotes the average over all measurements in each pixel, and $\hat{\alpha}_t$ is the estimated polarization angle for t -th measurement at each pixel, which has small polarization angle error $\delta_t \equiv \hat{\alpha}_t - \alpha_t$. We also define

$$\hat{\Psi}_t^{\pm 1} = \frac{1 - e^{\mp 4i\hat{\alpha}_t} \langle e^{\pm 4i\hat{\alpha}_t} \rangle_{\text{pix}}}{1 - \langle e^{\mp 4i\hat{\alpha}_t} \rangle_{\text{pix}} \langle e^{\pm 4i\hat{\alpha}_t} \rangle_{\text{pix}}}. \quad (31)$$

The subscripts, + and -, in Ξ^s are the total and difference of anisotropies obtained from the two detectors:

$$\Xi_+^{(s)} = \frac{\Xi_1^{(s)} \pm \Xi_2^{(s)}}{2}. \quad (32)$$

Note that, if the temperature and polarization anisotropies are measured only one time for each pixel, the quantities, $\hat{\Psi}_t^{\pm 1}$, in Eqs. (29) and (30) should be replaced with unity.

With Eqs. (29) and (30), taking into account the polarization angle involved in $\Xi^{(s)}$, the measured temperature and polarization in Fourier space are given by

$$\begin{aligned} \hat{X}_\ell &= \sum_{n=-\infty}^{\infty} \sum_{p=0,\pm 1} \sum_{Y=\Theta,E,B} \int \frac{d^2\mathbf{L}}{(2\pi)^2} \\ &\quad \times \mathcal{B}_{L,(n,p)}^{(XY)} \tilde{Y}_L \psi_{L'}^{(n,p)} e^{i n \varphi_{L,L'}} e^{2i p \varphi_{L,\ell}}, \end{aligned} \quad (33)$$

where $X = \Theta, E$ or B , the quantities, $\psi_{L'}^{(n,p)}$ ($p = 0, \pm 1$), are defined as the Fourier transform of the following quantities:

$$\psi_{L'}^{(n,p)}(\hat{\mathbf{n}}_i) = \langle e^{-i n \hat{\alpha}_t(\hat{\mathbf{n}}_i)} e^{i(n+2p)\delta_t(\hat{\mathbf{n}}_i)} \hat{\Psi}_t^p(\hat{\mathbf{n}}_i) \rangle_{\text{pix}} e^{i n \varphi_{L'}}, \quad (34)$$

with $\hat{\Psi}_t^0 = 1$. Note that $\psi_{L'}^{(n,p)}$ is the spin- $(-n)$ transform of spin- $(-n)$ quantity, $\langle e^{-i n \hat{\alpha}_t(\hat{\mathbf{n}}_i)} \hat{\Psi}_t^p(\hat{\mathbf{n}}_i) \rangle_{\text{pix}}$, in the limit of $\delta_i = 0$ for all measurements. The coefficients, $\mathcal{B}_{L,(n,p)}^{(ZZ')}$, are given by

$$\begin{aligned} \mathcal{B}_{L,(n,0)}^{(\Theta\Theta)} &= b_{L,n}^+ \\ \mathcal{B}_{L,(n,0)}^{(\Theta E)} &= -\frac{b_{L,n+2}^- + b_{L,n-2}^-}{2} \\ \mathcal{B}_{L,(n,0)}^{(\Theta B)} &= i \frac{b_{L,n+2}^- - b_{L,n-2}^-}{2} \\ \mathcal{B}_{L,(n,\pm 1)}^{(E\Theta)} &= -b_{L,n\pm 2}^- \\ \mathcal{B}_{L,(n,\pm 1)}^{(EE)} &= \frac{b_{L,n}^+ + b_{L,n\pm 4}^+}{2} \\ \mathcal{B}_{L,(n,\pm 1)}^{(EB)} &= \pm i \frac{b_{L,n}^+ - b_{L,n\pm 4}^+}{2} \\ \mathcal{B}_{L,(n,\pm 1)}^{(BY)} &= \mp i \mathcal{B}_{L,(n,\pm 1)}^{(EY)}, \end{aligned} \quad (35)$$

where $b_{L,n}^{\pm}$ is the total and difference of beam transfer functions for two detectors:

$$b_{L,n}^{\pm} = \frac{b_{L,n}^{(1)} \pm b_{L,n}^{(2)}}{2}. \quad (36)$$

Note that, in full sky and only for temperature case, Eq. (33) is consistent with Hanson et al. (2010).

In Fourier space, we break $\psi_{L'}^{(n,p)}$ into constant and fluctuation pieces

$$\psi_{L'}^{(n,p)} = C^{(n,p)} \delta_{\ell=0} + (\psi_{L'}^{(n,p)})_{\text{ani}}, \quad (37)$$

with the assumption that $(\psi_{L'}^{(n,p)})_{\text{ani}}$ are small. Then, Eq. (33) is rewritten as

$$\begin{aligned} \hat{X}_\ell &= \sum_{n=-\infty}^{\infty} \sum_{p=0,\pm 1} \sum_{Y=\Theta,E,B} \left\{ \mathcal{B}_{L,(n,p)}^{(XY)} \tilde{Y}_L e^{i n \varphi_{L,\ell}} C^{(n,p)} \right. \\ &\quad \left. + \int \frac{d^2\mathbf{L}}{(2\pi)^2} \mathcal{B}_{L,(n,p)}^{(XY)} \tilde{Y}_L (\psi_{L'}^{(n,p)})_{\text{ani}} e^{i n \varphi_{L,L'}} e^{2i p \varphi_{L,\ell}} \right\}, \end{aligned} \quad (38)$$

For realistic cases, $b_{L,n}^+/b_{L,0}^+ \ll 1$ for $n \neq 0$, $b_{L,n}^- \ll b_{L,n}^+$ and $\delta_i \ll 1$. Under these approximations, the dominant term in the first term of Eq. (38) becomes $b_{L,0}^+ X_\ell$. Assuming that $b_{L,0}^+ = 1$, the convolution in Eq. (38) leads to an off-diagonal covariance given by

$$\begin{aligned} \langle \hat{X}_L \hat{Y}_{L'} \rangle &= \sum_{n \neq 0} \sum_{p=0,\pm 1} f_{\ell,L}^{\psi^{(n,p)},(XY)} (\psi_{L'}^{(n,p)})_{\text{ani}} \\ &\quad + \mathcal{O}[(\psi^{(n,p)})_{\text{ani}}^2], \end{aligned} \quad (39)$$

where the weight functions are summarized in Table 3. Since $\psi^{(n,p)}$ is a spin- n quantities, it is useful to define a rotational-invariant quantities:

$$\psi_{\ell}^{(n,e)} = \psi_{\ell}^{(-n,0)} + (-1)^n \psi_{\ell}^{(n,0)}, \quad (40)$$

$$\psi_{\ell}^{(n,b)} = -i[\psi_{\ell}^{(-n,0)} - (-1)^n \psi_{\ell}^{(n,0)}], \quad (41)$$

$$\psi_{\ell}^{(n,\varepsilon)} = \psi_{\ell}^{(-n,+1)} + (-1)^n \psi_{\ell}^{(n,-1)}, \quad (42)$$

$$\psi_{\ell}^{(n,\beta)} = -i[\psi_{\ell}^{(-n,+1)} - (-1)^n \psi_{\ell}^{(n,-1)}], \quad (43)$$

where the above quantities satisfy $(\psi_{\ell}^{(n,\varepsilon)})^* = \psi_{-\ell}^{(n,\varepsilon)}$ and $(\psi_{\ell}^{(n,\beta)})^* = \psi_{-\ell}^{(n,\beta)}$. The corresponding weight function is then given as

$$f_{\ell L}^{(n,e)} = f_{\ell L}^{(-n,0)} + (-1)^n f_{\ell L}^{(n,0)}, \quad (44)$$

$$f_{\ell L}^{(n,b)} = -i[f_{\ell L}^{(-n,0)} - (-1)^n f_{\ell L}^{(n,0)}], \quad (45)$$

$$f_{\ell L}^{(n,\varepsilon)} = f_{\ell L}^{(-n,+1)} + (-1)^n f_{\ell L}^{(n,-1)}, \quad (46)$$

$$f_{\ell L}^{(n,\beta)} = -i[f_{\ell L}^{(-n,+1)} - (-1)^n f_{\ell L}^{(n,-1)}], \quad (47)$$

For $b_{L,0}^+ \neq 1$, we can utilize $f_{\ell,L}^{\psi^{(n,p)},(XY)}/(b_{L,0}^+ b_{L',0}^+)$ for the weight function. Note that the above derivations cover simpler cases; if the beam of two detectors are the same, $b^- = 0$, with Gaussian shape, $b_{L,n} \propto \delta_{n,0}$, and $\hat{\alpha}_t$ is the same for all measurements, we obtain $\hat{\Xi}^{(\pm 2)}(\hat{\mathbf{n}}) = \Xi^{(\pm 2)}(\hat{\mathbf{n}}) e^{\pm 2i\delta(\hat{\mathbf{n}})}$. We also note that, for only temperature case, the results are consistent with our previous work.

3.2 Mean-field biases

All of the above contaminations lead to the mean-field bias for lensing estimator, $\hat{x}_\ell^{(XY)}$. Omitting the subscript (XY) ,

the mean-field biases are given by

$$\begin{aligned}\langle \hat{x}_\ell \rangle &= A_\ell^{xx} \int \frac{d^2 \mathbf{L}}{(2\pi)^2} g_{\ell, \mathbf{L}}^x \langle \bar{X}_L \bar{Y}_{L'} \rangle \\ &= A_\ell^{xx} \int \frac{d^2 \mathbf{L}}{(2\pi)^2} \sum_y g_{\ell, \mathbf{L}}^x f_{\ell, \mathbf{L}}^y y_\ell \\ &= \sum_y R_\ell^{xy} y_\ell,\end{aligned}\quad (48)$$

where $y = M, S$ or $\psi^{(n,p)}$, and we define the response function R_ℓ and normalization A_ℓ as:

$$R_\ell^{xy} = \frac{A_\ell^{xx}}{A_\ell^{xy}}; \quad A_\ell^{xy} = \left\{ \int \frac{d^2 \mathbf{L}}{(2\pi)^2} g_{\ell, \mathbf{L}}^x f_{\ell, \mathbf{L}}^y \right\}^{-1}. \quad (49)$$

3.3 Bias-hardened estimator

Estimators which are bias-hardened against the effects above may be constructed analogously to the temperature case, i.e., we first construct a naive estimator for a given effect y as

$$\hat{y}_\ell = A_\ell^{yy} \int \frac{d^2 \mathbf{L}}{(2\pi)^2} g_{\ell, \mathbf{L}}^y \bar{X}_L \bar{Y}_{L'}, \quad (50)$$

where $g_{\ell, \mathbf{L}}^y$ and A_ℓ^{yy} are defined as Eq. (11) and (12), respectively, but using the weight function, $f_{\ell, \mathbf{L}}^{y, (XY)}$, instead of the lensing weight function, $f_{\ell, \mathbf{L}}^{x, (XY)}$ ($x = \phi, \varpi$). This estimator for y_ℓ is in turn biased by lensing. We may then obtain a bias-hardened estimator as

$$\hat{x}_\ell^{(\text{BHE})} \equiv \sum_y \{ \mathbf{R}_\ell^{-1} \}^{x,y} \hat{y}_\ell. \quad (51)$$

4 DEMONSTRATION OF BIAS-HARDENED ESTIMATOR FOR MEAN-FIELD BIAS

In this section, we discuss whether the bias-hardened estimator for lensing fields can be used as a cross-check for conventional estimator. For this purpose, we first compute the case where the mean field is generated only from the effect of masking. One concern here is the validity of linear-order approximation. That is, to derive bias-hardened estimator, we have ignored any higher-order terms of M_L (and, of course, for other non-lensing fields).

4.1 Simulated Maps and Analysis

We use simulated polarization maps produced using methods similar to our previous work (Namikawa et al. 2013). For lensing reconstruction, we use 100 realizations of lensed Stokes Q and U maps, simulated on a $5 \times 5 \text{ deg}^2$ patch. The details of the method used to generate these lensed maps are described in Appendix B. To simulate the masking of point sources we create masks by cutting 200 regions of randomly located $10' \times 10'$ squares. Note that the area covered by the point-source masks is $\sim 5 \%$ of total area, and the percentage roughly corresponds to that used in the SPT polarization analysis (Hanson et al. 2013). To consider experiments with high-angular resolution such as SPTpol, PolarBear and ACTPol, as well as to avoid contamination by the Sunyaev-Zel'dovich effect (Zel'dovich & Sunyaev 1969) and

unresolved point sources, we assume a delta function instrumental beam. The E and B modes multipoles are used at $2 \leq \ell \leq 3000$. We assume homogeneous map noise, with a level of $0.01 \mu\text{K-arcmin}$. Note that, even in the presence of an inhomogeneous noise, by combining the bias-hardened estimator described in Sec. 3.1.2, the mean field due to inhomogeneous noise would be reduced as already applied to the lensing reconstruction with Planck temperature map (Planck Collaboration 2013b), and the qualitative result would be similar to that obtained in this paper.

4.2 Filtering

For the conventional estimator approach, we experiment with the following filtering techniques to suppress the mask-mean field: apodization of the survey boundary and C^{-1} filtering for the point-source holes.

4.2.1 Apodization window function

In our analysis, we use the following analytic apodization function whose value and derivatives are zero at the boundaries of the survey region:

$$W(x, y; s_0) = w(x; s_0) w(y; s_0) M(x, y), \quad (52)$$

where $w(s; s_0)$ is a sine apodization function given by

$$w(s; s_0) = \begin{cases} 1 & |s| < as_0 \\ \frac{1 - |s|/a}{1 - s_0} - \frac{1}{2\pi} \sin\left(2\pi \frac{1 - |s|/a}{1 - s_0}\right) & as_0 \leq |s| < a \\ 0 & a \leq |s| \end{cases}, \quad (53)$$

and $M(x, y)$ represents the point-source mask, i.e., 0 at the presence of (resolved) point sources, and otherwise 1. The parameter, s_0 , indicates the width of the region where the apodization is applied.

4.2.2 C^{-1} filtering

The minimum-variance filtering which emerges from likelihood-based derivations of lensing estimators is known as C^{-1} filtering. The inverse-variance filtered Fourier modes, $\bar{\mathbf{X}}_\ell = (E_\ell, B_\ell)$, are obtained by solving

$$\left[1 + \mathbf{C}^{1/2} \mathbf{N}^{-1} \mathbf{C}^{1/2} \right] (\mathbf{C}^{1/2} \bar{\mathbf{X}}) = \mathbf{C}^{1/2} \mathbf{N}^{-1} \hat{\mathbf{X}}, \quad (54)$$

where $\bar{\mathbf{X}}$ is a vector whose components are \bar{X}_ℓ , \mathbf{C} is the covariance of the CMB anisotropies with

$$\{ \mathbf{C} \}_{\ell_i, \ell_j} = \delta_{\ell_i - \ell_j} \begin{pmatrix} C_{\ell_i}^{EE} & 0 \\ 0 & C_{\ell_i}^{BB} \end{pmatrix}, \quad (55)$$

and $\mathbf{N} = \langle \mathbf{n}^\dagger \mathbf{n} \rangle$ is the covariance matrix for the instrumental noise. The noise covariance matrix in Fourier space is obtained from that in real space as

$$\mathbf{N}^{-1} = \mathbf{Y}^\dagger \bar{\mathbf{N}}^{-1} \mathbf{Y}, \quad (56)$$

where the pointing matrix, \mathbf{Y} , is defined by

$$\{ \mathbf{Y} \}_{\hat{\mathbf{n}}_i, \ell_j} = \exp(i \hat{\mathbf{n}}_i \cdot \ell_j) \exp(-2\varphi_{\ell_j}) \begin{pmatrix} 1 & i \\ i & -1 \end{pmatrix}. \quad (57)$$

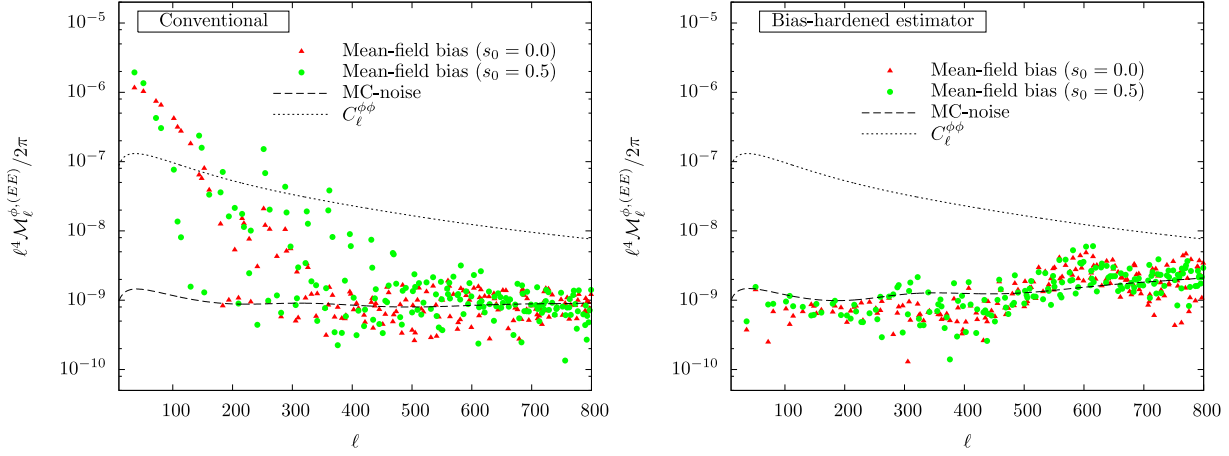


Figure 1. *Left:* Mean-field power spectrum for the gradient-mode EE estimator, $\mathcal{M}_\ell^{\phi, (EE)}$, estimated with 100 lensed simulated maps. The left panel shows results with the conventional estimator, varying the apodization parameter, s_0 , as 0.0 and 0.5. The Monte-Carlo noise floors (dashed line) are shown comparing with the mean-field power spectrum. The theoretical lensing power spectrum is also shown as a solid gray line. Note that the reconstruction is performed on $(5 \text{ deg})^2$, with E -mode multipoles ranges of, $2 \leq \ell \leq 3000$. *Right:* Same as left panel but with the bias-hardened estimator.

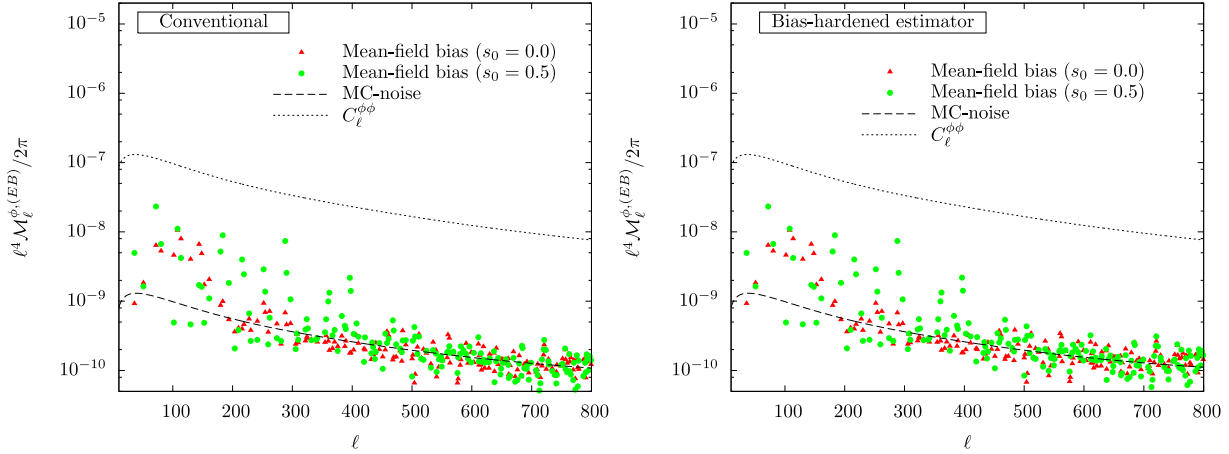


Figure 2. Same as Fig. 1, but for the EB case.

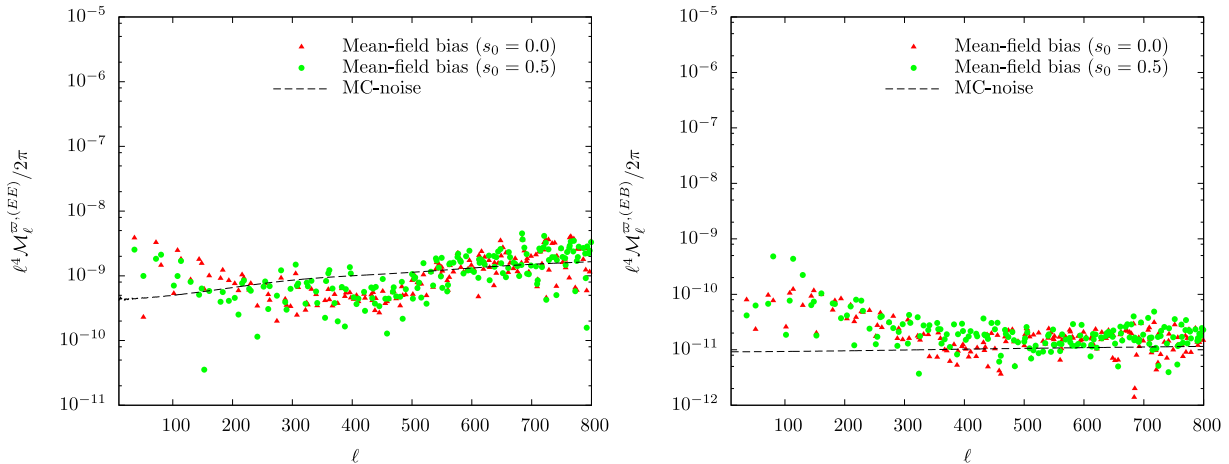


Figure 3. Mean-field power spectrum for curl modes with EE (left) and EB (right) estimators, respectively. The Monte-Carlo noise floors are shown with dashed lines.

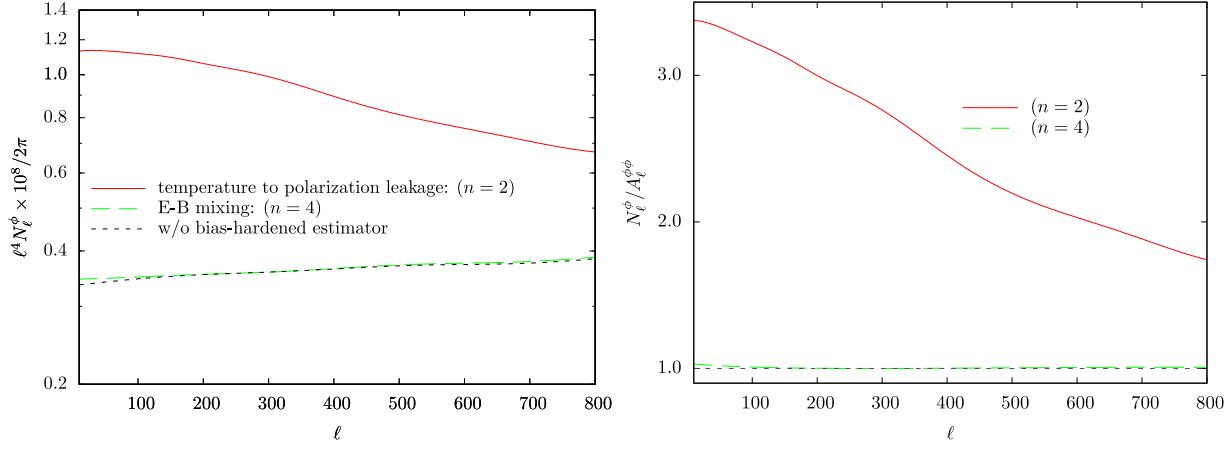


Figure 4. *Left:* Comparison of the noise level of lensing reconstruction between the case with and without the bias-hardened estimator for EB case. The noise level of the bias-hardened estimator, N_ℓ^ϕ , is computed from Eq. (67). The labels, $n = 2$ and $n = 4$, denote the temperature to polarization leakage, and E - B mixing by the rotation of the coordinate system, respectively (see text for the definitions and details). *Right:* The ratio of the noise level described in the left panel compared to the case w/o the bias-hardened estimator, $N_\ell^\phi / A_\ell^{\phi\phi}$.

Note that the matrix in the above equation describes the transformation of $(E_\ell, B_\ell)^t$ to $(E_\ell + iB_\ell, E_\ell - iB_\ell)^t$. The mask is incorporated by setting the noise level of masked pixels to infinity, and therefore the inverse of the noise covariance in real space \overline{N}^{-1} to zero for masked pixels. The inversion of the matrix on the left-hand side of Eq. (54) can be numerically costly, but may be evaluated using conjugate descent with careful preconditioning (Smith et al. 2007). Since the mask mean-field due to the survey boundary remains after applying the C^{-1} filter, we additionally apply an apodizing function given by Eq. (53).

4.3 Mean-field bias due to masking

We now turn to discuss the mean-field bias generated by masking.

Given N realizations of estimator, $\hat{x}_\ell^{i,(XY)}$ ($i = 1, 2, \dots, N$), we define the mean-field power spectrum as

$$\mathcal{M}_\ell^{x,(XY)} = \frac{1}{W_4} \int \frac{d\varphi_\ell}{2\pi} \left| \frac{1}{N} \sum_{i=1}^N \hat{x}_\ell^{i,(XY)} \right|^2, \quad (58)$$

where the quantity W_4 is the normalization correction for effect of window function as

$$W_4 = \int d^2\hat{n} [W(\hat{n})]^4. \quad (59)$$

With N -realizations of CMB maps, the mean-field becomes (Benoit-Levy et al. 2013)

$$\mathcal{M}_\ell^{x,(XY)} \simeq \frac{1}{W_4} \int \frac{d\varphi_\ell}{2\pi} |\langle \hat{x}_\ell^{(XY)} \rangle|^2 + \frac{A_\ell^{xx,(XY)} + C_\ell^{xx}}{N}. \quad (60)$$

The resulting mask mean-field for $\hat{\phi}$ are shown in Figs. 1 and 2 for quadratic combination of EE and EB cases, respectively. We compare results between the case with and without the bias-hardened estimator for mitigating mask mean-field. We also vary the apodization parameter, s_0 , introduced in Eq. (53). The Monte-Carlo noise floor is the

second term of Eq. (60). For EE , the mask mean-field is large on large angular scales, and exceeds the expected lensing power. We can clearly see that the bias-hardened estimator works well to mitigate the mask mean-field. On the other hand, the EB estimator has small contributions to the mask mean-field. The reason is as follow. If we use the filtering methods, the quantity M_ℓ has value only around ~ 0 , and thus the mask-mean field, which is expressed as $R_\ell^{xM} M_\ell$, is significant only for ~ 0 . For EB estimator, however, the response function, R_ℓ^{xM} , given in Eq. (49), has the sine function involved in the weight function, $f_{\ell,L}^{x,(EB)}$, and goes to zero as $\rightarrow 0$, which is contrary to the case of EE estimator in which the weight function includes the cosine function instead of sine function. Note that the origin of the sine function in the weight function is the parity of EB cross-correlation, i.e., odd parity symmetry, as the weight function is given by Eq. (9). We have also checked that, since the behavior of the response function for ΘB is similar to that of EB , the mask mean-field is negligible for ΘB estimator. As expected, the mask mean-field on the curl mode shown in Fig. 3 would also be negligible for both EE and EB estimator.

The residual mean-field bias also affects on the power spectrum estimation through

$$\int \frac{d\varphi_\ell}{2\pi} |\hat{x}_\ell|^2 = \mathcal{M}_\ell^x + A_\ell^{xx} + C_\ell^{xx}. \quad (61)$$

The figure shows that, for EE , the conventional estimator generates a significant mask-mean field which exceeds the lensing power spectrum; the lensing power spectrum estimation could therefore suffer from uncertainties in the mean-field correction. On the other hand, the bias-hardened estimator significantly suppresses the mask-mean field which is below the lensing power spectrum.

4.4 Mean-field bias due to polarization angle

The mask-mean field for the EB estimator is negligible even for the case with a simple apodization function, however,

the mean-field biases can be generated from other sources such as polarization angle errors. Here, to see the potential of bias-hardened estimators to mitigate polarization angle systematics, we compute a rough estimation of the response function and degradation of noise level for EB estimator.

For a two-beam experiment, with $b^- \neq 0$ and $b_{L,n} \propto \delta_{n,0}$, as an example, we consider the following non-zero weight functions for EB estimator:

$$f_{\ell,L}^{\psi(\pm 2, \mp 1)} = \mp i e^{\pm 2i\varphi_{L',\ell}} b_{L,0}^- \tilde{C}_L^{\Theta E} \quad (62)$$

$$f_{\ell,L}^{\psi(\pm 4, \mp 1)} = \pm i e^{\pm 2i(\varphi_{L,\ell} + \varphi_{L',\ell})} (b_{L,0} \tilde{C}_L^{BB} + b_{L',0} \tilde{C}_{L'}^{EE}), \quad (63)$$

where we have omitted the label, (EB) , in the weight functions. Note that the cases with $(n, p) = (\pm 2, \mp 1)$ and $(\pm 4, \mp 1)$ denote the systematics due to temperature to polarization leakage and E-B modes mixing, respectively. In general, as an alternative to $\psi_{\ell}^{(n,p)}$, we can use the following quantities:

$$\psi_{\ell}^{(n,\varepsilon)} = \psi_{\ell}^{(-n,+1)} + (-1)^n \psi_{\ell}^{(n,-1)}, \quad (64)$$

$$\psi_{\ell}^{(n,\beta)} = -i[\psi_{\ell}^{(-n,+1)} - (-1)^n \psi_{\ell}^{(n,-1)}], \quad (65)$$

where the above quantities satisfy $(\psi_{\ell}^{(n,\varepsilon)})^* = \psi_{-\ell}^{(n,\varepsilon)}$ and $(\psi_{\ell}^{(n,\beta)})^* = \psi_{-\ell}^{(n,\beta)}$. The corresponding weight functions for $\psi_{\ell}^{(n,\varepsilon)}$ and $\psi_{\ell}^{(n,\beta)}$ are

$$\begin{aligned} f_{\ell,L}^{\psi(2,\varepsilon)} &= b_{L,0}^- \sin(2\varphi_{L',\ell}) \tilde{C}_L^{\Theta E}, \\ f_{\ell,L}^{\psi(2,\beta)} &= -b_{L,0}^- \cos(2\varphi_{L',\ell}) \tilde{C}_L^{\Theta E}, \\ f_{\ell,L}^{\psi(4,\varepsilon)} &= -\sin(2\varphi_{L,\ell} + 2\varphi_{L',\ell}) (b_{L,0} \tilde{C}_L^{BB} + b_{L',0} \tilde{C}_{L'}^{EE}), \\ f_{\ell,L}^{\psi(4,\beta)} &= \cos(2\varphi_{L,\ell} + 2\varphi_{L',\ell}) (b_{L,0} \tilde{C}_L^{BB} + b_{L',0} \tilde{C}_{L'}^{EE}). \end{aligned} \quad (66)$$

In our calculation, for simplicity, we assume $b_{L,0}^- \equiv \epsilon b_{L,0}$ and a top-hat function for $b_{L,0}$, i.e., $b_{L,0} = 1$ for $\ell \leq 3000$ and 0 otherwise, and also ignore \tilde{C}_L^{BB} in the above equation. Since the weight functions of $\psi_{\ell}^{(n,\beta)}$ is obtained only by replacing sine function in $f_{\ell,L}^{\psi(2,\varepsilon)}$ with cosine function, we expect that the amplitude of the noise level for $\psi_{\ell}^{(n,\beta)}$ would be not so different from that for $\psi_{\ell}^{(n,\varepsilon)}$, and we only focus on the case to mitigate $\psi_{\ell}^{(n,\varepsilon)}$ in the following calculations.

In the left panel of Fig. 4, we show the noise level for the bias-hardened estimator incorporating polarization angle systematics of $\psi_{\ell}^{(n,\varepsilon)}$. The noise level for the conventional approach corresponds to the normalization, A_{ℓ}^{ϕ} . On the other hand, with $n = 2$ and 4, the noise level for the bias-hardened estimator is given by

$$N_{\ell}^{\phi} = \frac{A_{\ell}^{\phi}}{1 - R_{\ell}^{\phi\psi(n,\varepsilon)} R_{\ell}^{\psi(n,\varepsilon)\phi}}, \quad (67)$$

where the response functions, $R_{\ell}^{\phi\psi(n,\varepsilon)}$ and $R_{\ell}^{\psi(n,\varepsilon)\phi}$, defined in Eq. (49), are computed with the weight functions given in Eq. (66). Note that the noise level does not depend on ϵ . We find that the noise level is not necessarily much larger using a bias-hardened estimator compared to the conventional approach. In the right panel, we also show the ratio of the case with the bias-hardened estimator to that with conventional estimator. We find that the degradation of noise level is only up to $\lesssim 1\%$ for $n = 4$, and by a factor of ~ 3 for $n = 2$. Our results imply that the bias-hardened estimator

is enough to utilize for a cross check of usual method for polarization angle systematics.

5 SUMMARY

We have discussed methods for mitigating the mean-field bias in the case of lensing reconstruction with CMB polarization. We first derived the mean-field bias generated from masking, inhomogeneous noise (and/or unresolved point sources), and polarization angle systematics associated with the asymmetric beam shape, in analogy to the temperature-only case. Then we performed numerical tests to see how significantly the mean-field bias from masking is mitigated with the bias-hardened estimator. We found that, for EE estimator, it is particularly useful for the reduction of the large-scale component of the mean-field. On the other hand, for the EB estimator, we found that the amplitude of mask mean-field is negligible compared to the lensing signal. The bias-hardened EB estimator, however, is useful for other potential sources of mean field, such as polarization angle systematics, and we showed that the increase of noise level is only up to 1% for $n = 4$ (E - B mixing), and by a factor of ~ 3 for $n = 2$ (temperature to polarization leakage), compared to the conventional approach.

ACKNOWLEDGMENTS

We greatly appreciate Duncan Hanson for valuable comments and helpful discussions. We are also grateful to Takashi Hamana and Takahiro Nishimichi for kindly providing the ray-tracing simulation code and the 2LPT code, and thank Ryo Nagata for useful comments. This work was supported in part by Grant-in-Aid for Scientific Research on Priority Areas No. 467 ‘‘Probing the Dark Energy through an Extremely Wide and Deep Survey with Subaru Telescope’’, by the MEXT Grant-in-Aid for Scientific Research on Innovative Areas (No. 22111501), by JSPS Grant-in-Aid for Research Activity Start-up (No. 80708511), and by JSPS Grant-in-Aid for Scientific Research (B) (No. 25287062) ‘‘Probing the origin of primordial mini-halos via gravitational lensing phenomena’’. Numerical computations were carried out on SR16000 at YITP in Kyoto University and Cray XT4 at Center for Computational Astrophysics, CfCA, of National Astronomical Observatory of Japan.

APPENDIX A: BIAS-HARDENED ESTIMATOR FOR LENSING POWER SPECTRUM

Here we present an optimal estimator for the lensing angular power spectrum, \tilde{C}_{ℓ}^{xx} , motivated by the maximum likelihood estimator for lensing trispectrum, as proposed in our previous work (Namikawa et al. 2013) where we considered the temperature anisotropies alone.

A1 Formalism

A1.1 Likelihood for lensed CMB anisotropies

Gaussian probability distribution function for temperature and polarization fields, $a = \Theta, E$ or B , whose covariance

matrix are $C^{a_{\ell}, b_{\ell'}} = \langle a_{\ell} b_{\ell'} \rangle$, is given by

$$P_g = \frac{1}{\sqrt{(2\pi)^N \det C}} \exp \left(-\frac{1}{2} \sum_{ab} \sum_{\ell, \ell'} a_{\ell} (C^{-1})^{a_{\ell}, b_{\ell'}} b_{\ell'} \right), \quad (\text{A1})$$

Since the lensed anisotropies, $\tilde{\Theta}, \tilde{E}, \tilde{B}$, are no longer the Gaussian fields, the perturbative expansion of the likelihood for the lensed anisotropies at leading order is given as (Amendola 1996; Regan et al. 2010)

$$P = \left[1 + \sum_{abcd} \sum_{\ell_i} \langle a_{\ell_1} b_{\ell_2} c_{\ell_3} d_{\ell_4} \rangle_c \frac{\partial}{\partial a_{\ell_1}} \frac{\partial}{\partial b_{\ell_2}} \frac{\partial}{\partial c_{\ell_3}} \frac{\partial}{\partial d_{\ell_4}} \right] P_g. \quad (\text{A2})$$

Here, we ignore the three-point correlation because this is generated due to the correlation between the integrated Sachs-Wolfe effect and lensing. The cumulant is given by

$$\begin{aligned} \langle a_{\ell_1} b_{\ell_2} c_{\ell_3} d_{\ell_4} \rangle_c &\simeq f_{\ell_{12}, \ell_1}^{ab} f_{\ell_{12}, \ell_3}^{cd} C_{|\ell_{12}|}^{\phi\phi} \delta_{\ell_{12}, -\ell_{34}} \\ &+ f_{\ell_{13}, \ell_1}^{ac} f_{\ell_{13}, \ell_2}^{bd} C_{|\ell_{13}|}^{\phi\phi} \delta_{\ell_{13}, -\ell_{24}} \\ &+ f_{\ell_{14}, \ell_1}^{ad} f_{\ell_{14}, \ell_2}^{bc} C_{|\ell_{14}|}^{\phi\phi} \delta_{\ell_{14}, -\ell_{23}}. \end{aligned} \quad (\text{A3})$$

Substituting Eq. (A3) into Eq. (A4), we obtain the probability distribution function for lensed CMB anisotropies. Note here that, we do not compute higher order terms of $C_{\ell}^{\phi\phi}$, since we use an approximation which requires the expression only up to the first order of $C_{\ell}^{\phi\phi}$.

A1.2 Derivative of probability distribution function

To obtain the maximum-likelihood point, we differentiate P with respect to C_{ℓ}^{xx} , and obtain

$$\frac{\partial P}{\partial C_{\ell}^{xx}} = \sum_{abcd} (\hat{f}_{\ell}^{ab} \hat{f}_{-\ell}^{cd} + \hat{f}_{\ell}^{ac} \hat{f}_{-\ell}^{bd} + \hat{f}_{\ell}^{ad} \hat{f}_{-\ell}^{bc}) P_g, \quad (\text{A4})$$

where the operator is defined as

$$\hat{f}_{\ell}^{ab} \equiv \sum_{\ell_1} f_{\ell, \ell_1}^{ab} \frac{\partial}{\partial a_{\ell_1}} \frac{\partial}{\partial b_{\ell-\ell_1}}. \quad (\text{A5})$$

We find that

$$\hat{f}_{\ell}^{ab} P_g = (\bar{x}_{\ell}^{ab} - \langle \bar{x}_{\ell}^{ab} \rangle) P_g, \quad (\text{A6})$$

where we define the unnormalized estimator as

$$\bar{x}_{\ell}^{ab} = \sum_{\ell_1} f_{\ell, \ell_1}^{ab} \bar{a}_{\ell_1} \bar{b}_{\ell-\ell_1}, \quad (\text{A7})$$

with the inverse variance filtered multipoles as $\bar{a}_{\ell} = \sum_{a', \ell'} (C^{-1})^{a_{\ell} a'_{\ell'} b_{\ell} b'_{\ell'}}$. Operating $\hat{f}_{-\ell}^{cd}$ again to Eq. (A6), we obtain

$$\frac{1}{P_g} \hat{f}_{-\ell}^{cd} \hat{f}_{\ell}^{ab} P_g = \bar{x}_{\ell}^{ab, (C)} \bar{x}_{-\ell}^{cd, (C)} - n_{\ell}^{ab, cd}, \quad (\text{A8})$$

where the mean-field corrected estimator and its reconstruction noise bias are given by

$$\bar{x}_{\ell}^{ab, (C)} \equiv \bar{x}_{\ell}^{ab} - \langle \bar{x}_{\ell}^{ab} \rangle \quad (\text{A9})$$

$$\begin{aligned} n_{\ell}^{ab, cd} &\equiv \langle (\bar{x}_{\ell}^{a(1)b} + \bar{x}_{\ell}^{ab(1)}) (\bar{x}_{-\ell}^{c(1)d} + \bar{x}_{-\ell}^{cd(1)}) \rangle_{(1)} \\ &- \frac{1}{2} \langle (\bar{x}_{\ell}^{a(1)b(2)} + \bar{x}_{\ell}^{a(2)b(1)}) (\bar{x}_{-\ell}^{c(1)d(2)} + \bar{x}_{-\ell}^{c(2)d(1)}) \rangle_{(1), (2)}, \end{aligned} \quad (\text{A10})$$

where index (i) denotes the simulated maps obtained from i th set of Monte Carlo simulation, and $\langle \dots \rangle_{(i)}$ denotes the ensemble average for the i th set of Monte Carlo. Note here that $\langle n_{\ell}^{ab, cd} \rangle$ corresponds to the disconnected part of $\langle \bar{x}_{\ell}^{ab, (C)} \bar{x}_{-\ell}^{cd, (C)} \rangle$. We then obtain the derivative of a log-likelihood, $\mathcal{L} = \ln P$, as

$$\begin{aligned} \frac{\partial \mathcal{L}}{\partial C_{\ell}^{xx}} &= \frac{1}{P} \frac{\partial P}{\partial C_{\ell}^{xx}} \simeq \frac{1}{P_g} \frac{\partial P}{\partial C_{\ell}^{xx}} \\ &= \sum_{abcd} \left[\bar{x}_{\ell}^{ab, (C)} \bar{x}_{-\ell}^{cd, (C)} - n_{\ell}^{ab, cd} + (a \leftrightarrow c) + (a \leftrightarrow d) \right]. \end{aligned} \quad (\text{A11})$$

A1.3 Temperature

Here we first consider the case of temperature alone (or $a = b = c = d \equiv X$). With Eq. (A11), the derivative of a log-likelihood, $\mathcal{L} = \ln P$, is

$$\frac{\partial \mathcal{L}}{\partial C_{\ell}^{xx}} = 3[\langle \bar{x}_{\ell}^{(C)} \rangle^2 - n_{\ell}], \quad (\text{A12})$$

where we drop the index, X , in the unnormalized estimator and disconnected bias. Eq. (A12) motivates an unbiased estimator:

$$\hat{C}_{\ell}^{xx} = \left(\frac{A_{\ell}}{2} \right)^2 [\langle \bar{x}_{\ell}^{(C)} \rangle^2 - n_{\ell}] = |\hat{x}_{\ell}^{(C)}|^2 - \hat{n}_{\ell}, \quad (\text{A13})$$

where

$$\begin{aligned} \hat{x}_{\ell}^{(C)} &= \frac{A_{\ell}}{2} \sum_{\ell_1} f_{\ell, \ell_1} \bar{\Theta}_{\ell_1} \bar{\Theta}_{\ell-\ell_1} \\ \hat{n}_{\ell} &= 2[2\langle \hat{x}_{\ell}^{\Theta(1)\Theta} \hat{x}_{-\ell}^{\Theta(1)\Theta} \rangle_{(1)} - \langle \hat{x}_{\ell}^{\Theta(1)\Theta(2)} \hat{x}_{-\ell}^{\Theta(1)\Theta(2)} \rangle_{(1), (2)}]. \end{aligned} \quad (\text{A15})$$

The above equation coincides with Namikawa et al. (2013), and is generalized for the cases using only lensed E-/B-modes alone.

A1.4 Temperature and Polarizations

We now generalize the case including polarizations. Eq. (A11) implies that, for each combination of (a, b) and (c, d) , we can construct the lensing power spectrum estimator as

$$\hat{C}_{\ell}^{ab, cd} = \hat{x}_{\ell}^{ab, (C)} \hat{x}_{-\ell}^{cd, (C)} - \hat{n}_{\ell}^{ab, cd}, \quad (\text{A16})$$

where the first term is the power spectrum of the usual quadratic estimator but the second term is the estimator for the disconnected bias, $\hat{n}_{\ell}^{ab, cd}$, defined as

$$\begin{aligned} \hat{n}_{\ell}^{ab, cd} &= \langle (\hat{x}_{\ell}^{a(1)b} + \hat{x}_{\ell}^{ab(1)}) (\hat{x}_{-\ell}^{c(1)d} + \hat{x}_{-\ell}^{cd(1)}) \rangle_{(1)} \\ &- \frac{1}{2} \langle (\hat{x}_{\ell}^{a(1)b(2)} + \hat{x}_{\ell}^{a(2)b(1)}) (\hat{x}_{-\ell}^{c(1)d(2)} + \hat{x}_{-\ell}^{c(2)d(1)}) \rangle_{(1), (2)}, \end{aligned} \quad (\text{A17})$$

Denoting $\alpha, \beta = abcd$, an optimal estimator would be obtained by combining all combinations of $abcd$ as

$$\hat{C}_{\ell}^{xx} = N_{\ell}^{xx} \sum_{\alpha, \beta} \{ (N_{\ell}^{xx})^{-1} \}^{\alpha, \beta} \hat{C}_{\ell}^{\alpha}, \quad (\text{A18})$$

where the optimal noise level and noise covariance matrix are given by

$$N_{\ell}^{xx} \equiv \sum_{\beta, \beta'} \{ (N_{\ell}^{xx})^{-1} \}_{\beta, \beta'}; \quad \{ \mathbf{N}_{\ell} \}^{\alpha, \beta} = \langle \hat{C}_{\ell}^{\alpha} \hat{C}_{\ell}^{\beta} \rangle. \quad (\text{A19})$$

APPENDIX B: NUMERICAL SIMULATION OF LENSED CMB MAPS

In this section, we briefly present our procedure to prepare lensed CMB maps. Our procedure is same as for the lensed CMB temperature maps in our previous paper (Namikawa et al. 2013, Appendix A), but newly including the polarization fluctuations. We prepared lensed CMB maps as follows:

1) We obtain unlensed CMB temperature and polarization power spectra, $C_\ell^{\Theta\Theta}$, $C_\ell^{\Theta E}$ and C_ℓ^{EE} , with CAMB (Lewis et al. 2000).

2) We generate Gaussian temperature fluctuations Θ_ℓ in Fourier space, based on the input power spectrum $C_\ell^{\Theta\Theta}$. Then, we also generate polarization fluctuations $E_\ell = \sqrt{C_\ell^{EE} - (C_\ell^{\Theta E})^2 / C_\ell^{\Theta\Theta}} R_\ell + (C_\ell^{\Theta E} / C_\ell^{\Theta\Theta}) \Theta_\ell$ where R_ℓ is normalized Gaussian fields (with zero mean and unit variance). Then, the fluctuations of Θ_ℓ and E_ℓ satisfy the input power spectra. Here we assume the primordial B-mode is zero. By performing a Fourier transform on the fluctuations (Θ_ℓ and E_ℓ), we generate an unlensed CMB map. The map is a square of $\sqrt{4\pi}$ radian ($\simeq 203\text{deg}$) on a side. We prepare 100 such unlensed maps.

3) We make a lensed CMB map by remapping the unlensed map according to Eq.(1). Here, we perform the ray-tracing simulations to obtain the deflection angles. We used a publicly available code RAYTRIX (Hamana & Mellier 2001) which follows the multiple scattering. In the standard multiple lens plane algorithm, we divide the distance from the observer to the last scattering surface (LSS) into several equal intervals and then put lens planes in the every intervals. The light rays emitted from the observer are deflected in the every lens planes before reaching the LSS. We numerically solve the light-ray positions by solving the multi lens equation and finally obtain the angular position shifts on the LSS (See Namikawa et al. (2013), Appendix A, for detailed discussions). We checked that the power spectrum of the lensing potential agrees with the expectation from CAMB.

4) By repeating the procedures 1) to 3), we prepared 100 lensed CMB maps. Each map has an area of $10 \times 10 \text{deg}^2$ with 1024×1024 grids, and hence the resulting angular resolution is $10\text{deg}/1024 \simeq 0.6\text{arcmin}$. Note that, in our analysis of lensing reconstruction, we further cut the maps into $5 \times 5 \text{deg}^2$.

Fig. B1 shows the CMB power spectra calculated from the 100 lensed CMB maps. The upper, middle and lower panels are for the TE, EE and BB power spectrum, respectively. The dots with error bars are the mean and the dispersion calculated from the 100 realizations. We use $s_0 = 0.5$ for the apodization given in Eq. (53). Note that, in order to mitigate the effect of E-B mixing due to the survey boundary effect, we estimate the lensed E and B modes using “pure” E and B estimators (Smith & Zaldarriaga 2007). The red(black) symbols are the results for the lensed(unlensed) case. The solid curves are the theoretical prediction of CAMB. Our simulation results agree with the theoretical prediction very well.

REFERENCES

Abazajian K., et al., 2013, preprint (arXiv:1309.5383)

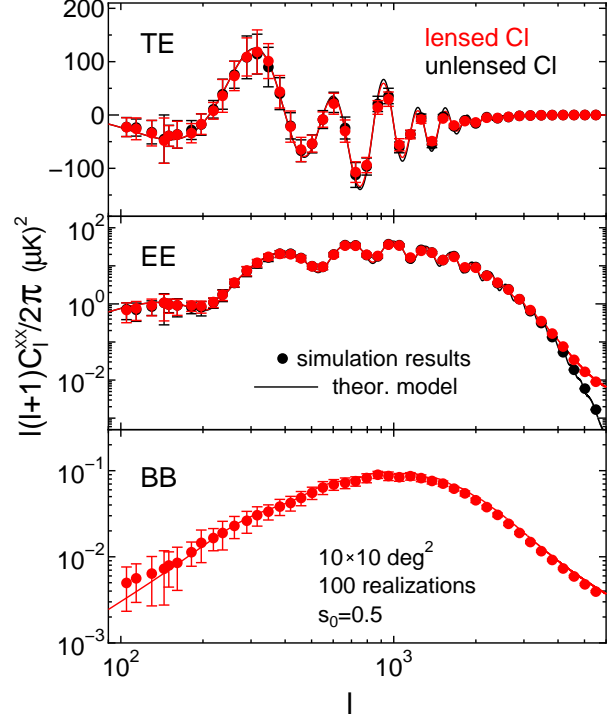


Figure B1. The lensed CMB power spectra for the TE(upper), EE(middle) and BB(lower). The red (black) symbols are the lensed (unlensed) power spectrum. The dots with error bars are our simulation results calculated from the 100 realizations of $10 \times 10 \text{deg}^2$ maps. The solid curves are the theoretical prediction of CAMB.

- Planck Collaboration, 2013a, preprint (arXiv:1303.5076)
 Planck Collaboration, 2013b, preprint (arXiv:1303.5077)
 Planck Collaboration, 2013c, preprint (arXiv:1303.5078)
 Amendola L., 1996, MNRAS, 283, 983
 Anderes E., 2013, Phys. Rev. D, 88, 083517
 Battye R. A., Moss A., 2013, preprint (arXiv:1308.5870)
 Benoit-Levy A., Dechelette T., Benabed K., Cardoso J.-F., Hanson D., Prunet S., 2013, Astronomy & Astrophysics, 555, 10
 Bleem L. et al., 2012, ApJ, 753, L9
 Carvalho C. S., Tereno I., 2011, Phys. Rev. D, 84, 063001
 Cooray A., Kamionkowski M., Caldwell R. R., 2005, Phys. Rev. D, 71, 123527
 Das S. et al., 2013, preprint (arXiv:1301.1037)
 Das S. et al., 2011, Phys. Rev. Lett., 107, 021301
 Geach J. et al., 2013, Astronomical Journal, 776, L41
 Hamana T., Mellier Y., 2001, MNRAS, 327, 169
 Hanson D., Challinor A., Efstathiou G., Bielewicz P., 2011, Phys. Rev. D, 83, 043005
 Hanson D. et al., 2013, Phys. Rev. Lett., 111, 141301
 Hanson D., Lewis A., Challinor A., 2010, Phys. Rev., D81, 103003
 Hanson D., Rocha G., Gorski K., 2009, MNRAS, 400, 2169
 Hirata C. M., Ho S., Padmanabhan N., Seljak U., Bahcall N. A., 2008, Phys. Rev. D, 78, 043520

- Hirata C. M., Seljak U., 2003, Phys. Rev. D, 68, 083002
- Holder G. et al., 2013, Astrophys.J., 771, L16
- Hu W., 2001, Phys. Rev. D, 64, 083005
- Hu W., Okamoto T., 2002, ApJ, 574, 566
- Jeong D., Komatsu E., Jain B., 2009, Phys. Rev. D, 80, 123527
- Joudaki S., Kaplinghat M., 2012, Phys. Rev. D, 86, 023526
- Kesden M., Cooray A., Kamionkowski M., 2002, Phys. Rev. Lett., 89, 011304
- Knox L., Song Y.-S., 2002, Phys. Rev. Lett., 89, 011303
- Lewis A., Challinor A., 2006, Phys. Rep., 429, 1
- Lewis A., Challinor A., Hanson D., 2011, JCAP, 1103, 018
- Lewis A., Challinor A., Lasenby A., 2000, ApJ, 538, 473
- Namikawa T., Hanson D., Takahashi R., 2013, MNRAS, 431, 609
- Namikawa T., Saito S., Taruya A., 2010, JCAP, 1012, 027
- Namikawa T., Yamauchi D., Taruya A., 2012, JCAP, 1201, 007
- Namikawa T., Yamauchi D., Taruya A., 2013, Phys. Rev. D, 88, 083525
- Okamoto T., Hu W., 2003, Phys. Rev. D, 67, 083002
- Perotto L., Bobin J., Plaszczyński S., Starck J.-L., Lavabre A., 2010, A&A, 519, A4
- Plaszczyński S., Lavabre A., Perotto L., Starck J.-L., 2012, A&A, 544, A27
- Regan D., Shellard E., Fergusson J., 2010, Phys. Rev. D, 82, 023520
- Seljak U., Zaldarriaga M., 1999, Phys. Rev. Lett., 82, 2636
- Sherwin B. D., Das S., 2010, preprint (arXiv:1011.4510)
- Sherwin B. D. et al., 2012, Phys. Rev. D, 86, 083006,
- Sherwin B. D. et al., 2011, Phys. Rev. Lett., 107, 021302
- Shimon M., Keating B., Ponthieu N., Hivon E., 2008, Phys. Rev. D, 77, 083003
- Smith K. M., 2006, New Astron.Rev., 50, 1025
- Smith K. M., Zahn O., Dorè O., 2007, Phys. Rev. D, 76, 043510
- Smith K. M., Zaldarriaga M., 2007, Phys. Rev. D, 76, 043001
- Takeuchi Y., Ichiki K., Matsubara T., 2012, Phys. Rev. D, 85, 043518
- van Engelen A. et al., 2012, Astrophys.J., 756, 142
- Wilkinson R. J., Lesgourgues J., Boehm C., 2013, preprint (arXiv:1309.7588)
- Yamauchi D., Namikawa T., Taruya A., 2012, JCAP, 1210, 030
- Yamauchi D., Namikawa T., Taruya A., 2013, JCAP, 1308, 051
- Zaldarriaga M., Seljak U., 1999, Phys. Rev. D, 59, 123507
- Zel'dovich Y., Sunyaev R., 1969, Astrophysics and Space Science, 4, 301